Low-latency Low-complexity Subspace Methods for mmWave MIMO-OFDM Channel Estimation

Mattia Cerutti[1], Monica Nicoli[1], Umberto Spagnolini[2]
[1]Dip. di Ingegneria Gestionale, [2]Dip. di Elettronica, Informazione e Bioingegneria, Politecnico di Milano, Italy

***Abstract*—Millimeter wave (mmWave) wideband channels in a multiple-input multiple-output (MIMO) transmission are described by a sparse set of impulse responses in the angle-delay, or space-time (ST), domain. In this paper we consider the problem of channel estimation and we discuss subspace methods which exploit the low-rank (LR) algebraic structure of the MIMO channel matrix and the related slowly- and fast-varying features (angles/delays of arrival and fading amplitudes, respectively). The main drawback of the optimal LR method is the excessively slow convergence to the mean square error lower bound for invariant angles/delay and time-varying fading. In this paper, new suboptimal LR techniques are proposed to reduce the complexity and accelerate the convergence. Numerical results show that the proposed methods closely approach the asymptotic bound with a number of slots that is two order of magnitudes lower than the optimal method, providing significant performance gains in realistic mmWave propagation scenarios.**

***Index Terms*—Channel estimation, low-rank subspace methods, mmWave, multiple-input-multiple-output (MIMO).**

I. Introduction

The escalating capacity demand of the fifth generation (5G) radio access networks has moved the research focus towards millimeter wave (mmWave) communications [1]–[4]. Unfortunately, the large spectral availability comes at the price of severe propagation losses and the use of large antenna arrays with sharp beamforming becomes mandatory to guarantee the coverage, leading to massive multiple-input multiple-output (MIMO) systems. Due to their sparse wideband structure, with few dominant paths typically clustered around the line-of-sight (LOS), multipath MIMO channels are described by a parsimonious set of parameters in the space-time (ST) domain, i.e. the domain of angles (of departure and arrival) and delays.

Training-based channel estimation and processing in mmWave MIMO involve several aspects that depend on the system configurations (see [4] for an overview) but all methods exploit the channel sparsity. In low-rank (LR) methods the sparsity is converted into a LR structure of the MIMO channel matrices, so that powerful algebraic methods can be applied, regardless of array configurations and calibration errors [5].

The complexity of transceivers can be reduced by hybrid analog/digital structures and specific solutions for mmWave channel estimation have been proposed for static environments [6]–[11]. However, mmWave environments are typically dynamic (at least for the fading fluctuations), and this is the context approached in this paper for MIMO channel estimation. The mmWave radio access has a fixed array unit with moving connected terminals. Movement of terminals is such that the ST features (angles of arrival/departure and delays) of the mmWave MIMO channel remain constant for several (say L) temporal intervals organized in time-slots. This invariance depends on the ST resolution of the MIMO system. Consider e.g. a vehicular LOS link with relative speed of 50 km/h and transmission frame of 1 ms (see [12] and [13]): angles and delays can be approximated as invariant for $L = 108$ slots when the link distance is 200 m, the antenna array resolution 1 deg and the bandwidth 200 MHz [14], [15].

This paper proposes to exploit the invariance of angles/delays and the related ST channel subspaces in mmWave MIMO orthogonal frequency division multiplexing (OFDM) systems. In this context, the LR methods [14], [16] can be straightforwardly extended. However a main drawback is the excessively slow convergence of the optimal method [16] that requires $L \gg 1000$ slots and contrasts with both the mmWave channel dynamics and the latency requirements (both calling for $L < 100$ slots). The main contribution of this paper with respect to the preliminary works [5], [14], [16], is that here the LR channel estimator is i) accelerated at the expenses of some sub-optimality and ii) tailored to mmWave MIMO-OFDM systems with realistic channel modeling. The proposed LR methods are sub-optimal but fast-converging, and with far lower complexity. The performances are evaluated in both simplified and realistic propagation scenarios, and compared with asymptotic lower bounds obtained as detailed in [17] by extending to MIMO-OFDM systems the bound in [5]. Numerical results show that the LR techniques closely approach the performance of the optimal method [16] with a number of slots two order of magnitudes lower, providing significant gains with respect to other LR methods in the literature.

II. System Model

We consider a mmWave MIMO OFDM system with N_{T} transmitting and N_{R} receiving antennas. The total number of OFDM subcarriers is denoted as K_{tot}, while K is the number of pilot subcarriers for channel estimation. $\mathbf{X}_{\ell}^{(n_{\mathrm{T}})} \in \mathbb{C}^{K\times 1}$ is the vector containing the pilot symbols transmitted over the K subcarriers from antenna $n_{\mathrm{T}} = 1, \ldots, N_{\mathrm{T}}$, within the OFDM block $\ell = 1, \ldots, L$, with index ℓ running over the blocks containing pilots (i.e., the training blocks). The cyclic prefix (CP) comprises $W - 1$ samples, where W denotes the maximum temporal support of the channel, with $K \geq W N_{\mathrm{T}}$.

At the receiver, after CP removal and computation of the K_{tot}-point discrete Fourier transform (DFT), the $K \times 1$

978-1-7281-5089-5/20/$31.00 ©2020 IEEE

complex baseband signal received by the $n_{\rm R}$-th antenna during the ℓ-th block is:

$$\mathbf{Y}_\ell^{(n_{\rm R})} = \sum\nolimits_{n_{\rm T}=1}^{N_{\rm T}} \mathrm{diag}\left(\mathbf{X}_\ell^{(n_{\rm T})}\right) \mathbf{H}_\ell^{(n_{\rm R},n_{\rm T})} + \mathbf{N}_\ell^{(n_{\rm R})}, \quad (1)$$

where $\mathbf{H}_\ell^{(n_{\rm R},n_{\rm T})} = \mathbf{F}\mathbf{h}_\ell^{(n_{\rm R},n_{\rm T})} \in \mathbb{C}^{K\times 1}$ is the channel for the link $(n_{\rm R}, n_{\rm T})$ in the frequency domain, obtained as the DFT of the corresponding $W \times 1$ time-domain channel $\mathbf{h}_\ell^{(n_{\rm R},n_{\rm T})} = [h_\ell^{(n_{\rm R},n_{\rm T})}(1) \cdots h_\ell^{(n_{\rm R},n_{\rm T})}(W)]^{\rm T}$. The DFT matrix has entries $[\mathbf{F}]_{k,w} = \exp(-j2\pi f_k w/K_{\rm tot})/\sqrt{K_{\rm tot}}$, with f_k denoting the frequency index of the k-th pilot subcarrier, $k = 0, \ldots, K-1$, and $w = 1, \ldots, W$. The w-th tap of the ST MIMO channel for the ℓ-th training block is denoted as $\mathbf{h}_\ell(w) \in \mathbb{C}^{N_{\rm R}\times N_{\rm T}}$, with $[\mathbf{h}_\ell(w)]_{n_{\rm R},n_{\rm T}} = h_\ell^{(n_{\rm R},n_{\rm T})}(w)$. The additive Gaussian noise-plus-interference signal $\mathbf{N}_\ell^{(n_{\rm R})} \in \mathbb{C}^{K\times 1}$ is assumed to be uncorrelated over the frequencies, i.e., $\mathbb{E}[\mathbf{N}_\ell^{(n_{\rm R})}\mathbf{N}_\ell^{(n_{\rm R})\rm H}] = K\sigma_n^2\mathbf{I}_K$, and spatially correlated due to the geometrical distribution of the interferers. By stacking column-wise the noise vectors into $\mathbf{N}_\ell = [\mathbf{N}_\ell^{(1)} \cdots \mathbf{N}_\ell^{(N_{\rm R})}]$, the noise-plus-interference spatial covariance is $\mathbf{Q} = \frac{1}{K}\mathbb{E}[\mathbf{N}_\ell^{\rm H}\mathbf{N}_\ell]$, which is to be estimated as the arrangement of the interferers is unknown in general.

A. MmWave Space-Time Channel

The mmWave channel is modelled as [18], [19]:

$$\mathbf{h}_\ell(w) = \sum\nolimits_{p=1}^{P} \alpha_{p,\ell}\mathbf{A}(\boldsymbol{\theta}_p)\, g((w-1)T - \tau_p), \quad (2)$$

where each path p has fading amplitude $\alpha_{p,\ell}$ and delay τ_p, while $g(\cdot)$ is the delayed impulse response of the cascade between the transmitter (TX) and receiver (RX) filters, sampled at symbol rate $1/T$. The matrix

$$\mathbf{A}(\boldsymbol{\theta}_p) = \mathbf{a}^{\rm RX}(\boldsymbol{\theta}_p^{\rm RX})\mathbf{a}^{\rm TX}(\boldsymbol{\theta}_p^{\rm TX})^{\rm T} \quad (3)$$

accounts for the RX and TX antenna array responses, $\mathbf{a}^{\rm RX}(\boldsymbol{\theta}_p^{\rm RX})$ and $\mathbf{a}^{\rm TX}(\boldsymbol{\theta}_p^{\rm TX})$. These responses depend on the azimuth (ϕ) and elevation (ψ) angles, for the arrival $\boldsymbol{\theta}_p^{\rm RX} = [\phi_p^{\rm RX}, \psi_p^{\rm RX}]$ and the departure, $\boldsymbol{\theta}_p^{\rm TX} = [\phi_p^{\rm TX}, \psi_p^{\rm TX}]$. Fast varying fading amplitudes $\alpha_{p,\ell}$ are block-dependent, while delays τ_p and angles $\boldsymbol{\theta}_p = [\boldsymbol{\theta}_p^{\rm TX}, \boldsymbol{\theta}_p^{\rm RX}]$ are assumed to be constant within L blocks.

The overall ST MIMO channel at block ℓ is arranged for analytical convenience into the $N_{\rm R}N_{\rm T} \times W$ matrix

$$\mathcal{H}_\ell = [\mathrm{vec}(\mathbf{h}_\ell(1)) \cdots \mathrm{vec}(\mathbf{h}_\ell(W))] = \mathcal{A}(\boldsymbol{\theta})\mathbf{D}_\ell\mathbf{G}(\tau)^{\rm T}, \quad (4)$$

where the $N_{\rm R}N_{\rm T} \times P$ complex matrix $\mathcal{A}(\boldsymbol{\theta}) = [\mathbf{a}(\boldsymbol{\theta}_1) \cdots \mathbf{a}(\boldsymbol{\theta}_P)]$ and the $W \times P$ real matrix $\mathbf{G}(\tau) = [\mathbf{g}(\tau_1) \cdots \mathbf{g}(\tau_P)]$ collect all the static ST channel components associated to the P paths, with $\mathbf{a}(\boldsymbol{\theta}_p) = \mathrm{vec}(\mathbf{A}(\boldsymbol{\theta}_p))$ and $\mathbf{g}(\tau_p) = [g(-\tau_p) \cdots g((W-1)T - \tau_p)]^{\rm T}$. The fading amplitudes $\mathbf{D}_\ell = \mathrm{diag}(\alpha_{1,\ell}, \ldots, \alpha_{P,\ell}) \in \mathbb{C}^{P\times P}$ are assumed to follow the wide-sense stationary uncorrelated scattering (WSSUS) model, and to be uncorrelated over blocks:

$$\mathbb{E}\left[\mathbf{D}_{\ell+m}\mathbf{D}_\ell^{\rm H}\right] = \boldsymbol{\Omega}\delta(m), \quad (5)$$

where $\boldsymbol{\Omega} = \mathrm{diag}(\Omega_1, \ldots, \Omega_P)$ and $\Omega_p > 0$ is the average power of the p-th path, normalized to have $\sum_{p=1}^{P}\Omega_p = 1$.

TABLE I: Channel Estimate Arrangements

Notation	Sample Ordering	Dimensions
$\hat{\mathbf{h}}_\ell$	Time, Space TX, Space RX	$WN_{\rm T}N_{\rm R} \times 1$
$\hat{\mathbf{h}}_\ell(w)$	Space RX, Space TX	$N_{\rm R} \times N_{\rm T}$
$\hat{\mathcal{H}}_\ell$	Space RX, Space TX, Time	$N_{\rm R}N_{\rm T} \times W$
$\hat{\boldsymbol{h}}_\ell$	Space RX, Space TX, Time	$N_{\rm R}N_{\rm T}W \times 1$

B. Pre-processing for ST Channel Estimation

Model (1) is rearranged to isolate the temporal channel responses as:

$$\mathbf{Y}_\ell^{(n_{\rm R})} = \mathbf{B}_\ell\mathbf{h}_\ell^{(n_{\rm R})} + \mathbf{N}_\ell^{(n_{\rm R})}, \quad (6)$$

where the $K \times WN_{\rm T}$ matrix $\mathbf{B}_\ell = [\mathrm{diag}(\mathbf{X}_\ell^{(1)})\mathbf{F} \cdots \mathrm{diag}(\mathbf{X}_\ell^{(N_{\rm T})})\mathbf{F}]$ collects the $N_{\rm T}$ training matrices, and the $WN_{\rm T} \times 1$ vector $\mathbf{h}_\ell^{(n_{\rm R})} = [\mathbf{h}_\ell^{(n_{\rm R},1)\rm T} \cdots \mathbf{h}_\ell^{(n_{\rm R},N_{\rm T})\rm T}]^{\rm T}$ the $N_{\rm T}$ channel impulse responses. The conventional approach for the estimation of $\mathbf{h}_\ell^{(n_{\rm R})}$ from (6) is the unconstrained maximum likelihood (ML) estimate, here referred to as full rank (FR) method:

$$\hat{\mathbf{h}}_\ell^{(n_{\rm R})} = \mathbf{B}_\ell^\dagger\mathbf{Y}_\ell^{(n_{\rm R})} = \mathbf{h}_\ell^{(n_{\rm R})} + \mathbf{B}_\ell^\dagger\mathbf{N}_\ell^{(n_{\rm R})}, \quad (7)$$

with $\mathbf{B}_\ell^\dagger = (\mathbf{B}_\ell^{\rm H}\mathbf{B}_\ell)^{-1}\mathbf{B}_\ell^{\rm H}$. This estimate is known to be unbiased with variance minimized by adopting equally spaced, equally powered, and orthogonal pilot sequences $\mathbf{X}_\ell^{(n_{\rm T})}$ with correlation matrix $\mathbf{R}_{\mathbf{BB}} = \mathbf{B}_\ell^{\rm H}\mathbf{B}_\ell = K\sigma_x^2\mathbf{I}_{N_TW}$ [20]. The noise spatial covariance estimate is obtained as:

$$\hat{\mathbf{Q}} = \frac{1}{KL}\sum\nolimits_{\ell=1}^{L}\hat{\mathbf{N}}_\ell^{\rm H}\hat{\mathbf{N}}_\ell, \quad (8)$$

from the residual signals $\hat{\mathbf{N}}_\ell^{(n_{\rm R})} = \mathbf{Y}_\ell^{(n_{\rm R})} - \mathbf{B}_\ell\hat{\mathbf{h}}_\ell^{(n_{\rm R})}$ aggregated over the antennas into $\hat{\mathbf{N}}_\ell = [\hat{\mathbf{N}}_\ell^{(1)} \cdots \hat{\mathbf{N}}_\ell^{(N_{\rm R})}]$.

Throughout the paper, we will use different rearrangements of the channel estimate as summarized in Table I. More specifically, being $\hat{h}_\ell^{(n_{\rm R},n_{\rm T})}(w) = [\hat{\mathbf{h}}_\ell^{(n_{\rm R})}]_{(n_{\rm T}-1)W+w}$ the w-th tap for link $(n_{\rm R}, n_{\rm T})$, we denote as $\hat{\mathbf{h}}_\ell(w)$ the $N_{\rm R} \times N_{\rm T}$ matrix collecting the w-th taps for the $N_{\rm R}N_{\rm T}$ MIMO links and as $\hat{\mathcal{H}}_\ell$ the whole $N_{\rm R}N_{\rm T} \times W$ doubly-space time matrix aggregating all taps, according to the channel arrangements in (2) and (4). The following equivalences hold:

$$\hat{h}_\ell^{(n_{\rm R},n_{\rm T})}(w) = \left[\hat{\mathbf{h}}_\ell(w)\right]_{n_{\rm R},n_{\rm T}} = \left[\hat{\mathcal{H}}_\ell\right]_{(n_{\rm T}-1)N_{\rm R}+n_{\rm R},w}. \quad (9)$$

To conclude, we define the vector collecting all the estimate samples over, respectively, time, the TX space and the RX space domains as $\hat{\mathbf{h}}_\ell = [\hat{\mathbf{h}}_\ell^{(1)\rm T} \cdots \hat{\mathbf{h}}_\ell^{(N_{\rm R})\rm T}]^{\rm T} \in \mathbb{C}^{WN_{\rm T}N_{\rm R}\times 1}$, with covariance $\mathbf{C} = \mathrm{cov}[\hat{\mathbf{h}}_\ell] = \mathbf{Q} \otimes \mathbf{R}_{\rm BB}^{-1}$. We will also use a permutation of this vector where the ordering is, respectively, according to the RX space, TX space and time domains as $\hat{\boldsymbol{h}}_\ell = \mathrm{vec}(\hat{\mathcal{H}}_\ell) \in \mathbb{C}^{N_{\rm R}N_{\rm T}W\times 1}$, with covariance $\boldsymbol{C} = \mathrm{cov}[\hat{\boldsymbol{h}}_\ell]$.

III. Low-Rank Channel Estimation

The mmWave MIMO wireless channel is sparse and the conventional estimate (7) is extremely noisy, especially in massive ST settings. To reduce the errors we propose to exploit the invariance of the directions of arrival/departure

TABLE II: Channel Sample Correlations

Correlation $\tilde{\mathbf{R}}$	Rank r	Dim.
$\tilde{\mathbf{R}}_{\mathrm{ST}} = \frac{1}{L}\sum_{\ell} \tilde{\boldsymbol{h}}_\ell \tilde{\boldsymbol{h}}_\ell^{\mathrm{H}}$	$r = \mathrm{rank}(\mathbf{O})$	$N_{\mathrm{R}}N_{\mathrm{T}}W$
$\tilde{\mathbf{R}}_{\mathrm{S}} = \frac{1}{L}\sum_{\ell} \tilde{\mathcal{H}}_\ell \tilde{\mathcal{H}}_\ell^{\mathrm{H}}$	$r_{\mathrm{S}} = \mathrm{rank}(\mathcal{A})$	$N_{\mathrm{R}}N_{\mathrm{T}}$
$\tilde{\mathbf{R}}_{\mathrm{T}} = \frac{1}{L}\sum_{\ell} \tilde{\mathcal{H}}_\ell^{\mathrm{H}} \tilde{\mathcal{H}}_\ell$	$r_{\mathrm{T}} = \mathrm{rank}(\mathbf{G})$	W
$\tilde{\mathbf{R}}_{\mathrm{S,TX}} = \frac{1}{L}\sum_{\ell,w} \tilde{\mathbf{h}}_\ell^{\mathrm{H}}(w) \tilde{\mathbf{h}}_\ell(w)$	$r_{\mathrm{S,TX}} = \mathrm{rank}(\mathbf{A}^{\mathrm{TX}})$	N_{T}
$\tilde{\mathbf{R}}_{\mathrm{S,RX}} = \frac{1}{L}\sum_{\ell,w} \tilde{\mathbf{h}}_\ell(w) \tilde{\mathbf{h}}_\ell^{\mathrm{H}}(w)$	$r_{\mathrm{S,RX}} = \mathrm{rank}(\mathbf{A}^{\mathrm{RX}})$	N_{R}

(DOA/DOD) and the delays of the propagation paths, to enable the identification of the LR algebraic structure of the multipath channel: rather than estimating DOD/DOA and delays based on a parametric model, the proposed LR methods describe the multipath components in terms of ST-invariant subspaces and estimate the channel by filtering the FR estimate through a set of ST projections. In this way, they avoid a joint angle and delay estimation which is computationally expensive and highly sensitive to antenna calibration. The LR channel modeling and the estimators are detailed in the following.

A. LR Algebraic Channel Structure

To highlight the relevant parameters and isolate the slowly-varying ones from the fast-varying terms, we consider the vectorized ST channel $\boldsymbol{h}_\ell = \mathrm{vec}\,(\mathcal{H}_\ell) \in \mathbb{C}^{N_{\mathrm{R}}N_{\mathrm{T}}W\times 1}$:

$$\boldsymbol{h}_\ell = \sum\nolimits_{p=1}^{P} \underbrace{\left(\mathbf{g}\left(\tau_p\right) \otimes \mathbf{a}\left(\boldsymbol{\theta}_p\right)\right)}_{\mathbf{o}_p} \alpha_{p,\ell} = \mathbf{O}\left(\boldsymbol{\tau},\boldsymbol{\theta}\right)\boldsymbol{\alpha}_\ell, \quad (10)$$

where $\mathbf{O}\left(\boldsymbol{\tau},\boldsymbol{\theta}\right) = [\mathbf{o}_1 \cdots \mathbf{o}_P] \in \mathbb{C}^{N_{\mathrm{R}}N_{\mathrm{T}}W\times P}$ collects the block-invariant ST signatures of the P paths (depending on angles and delays), while $\boldsymbol{\alpha}_\ell = [\alpha_{1,\ell}\cdots\alpha_{P,\ell}]^{\mathrm{T}} \in \mathbb{C}^{P\times 1}$ embeds the block-varying amplitudes. According to the WSSUS assumption, we define the ST channel correlation matrix $\mathbf{R}_{\mathrm{ST}} = \mathbb{E}[\boldsymbol{h}_\ell \boldsymbol{h}_\ell^{\mathrm{H}}] \in \mathbb{C}^{N_{\mathrm{R}}N_{\mathrm{T}}W\times N_{\mathrm{R}}N_{\mathrm{T}}W}$, and we denote with

$$r = \mathrm{rank}\left(\mathbf{O}\left(\boldsymbol{\tau},\boldsymbol{\theta}\right)\right) \leq \min\left(N_{\mathrm{R}}N_{\mathrm{T}}W, P\right) \quad (11)$$

the number of resolvable paths given the system resolution (i.e., the antenna array aperture and the system bandwidth). Based on the LR constraint (11), we can rewrite the channel (10) according to the joint space-time (JST) LR model [16]

$$\boldsymbol{h}_\ell = \mathbf{U}_{\mathrm{ST}}\boldsymbol{\gamma}_\ell, \quad (12)$$

where $\mathbf{U}_{\mathrm{ST}} \in \mathbb{C}^{N_{\mathrm{R}}N_{\mathrm{T}}W\times r}$ is a block-independent full-rank matrix that collects the r eigenvectors of $\mathbf{R}_{\mathrm{ST}}$ and spans the invariant ST subspace $\mathcal{R}(\mathbf{U}_{\mathrm{ST}}) = \mathcal{R}(\mathbf{O}(\boldsymbol{\tau},\boldsymbol{\theta}))$, while $\boldsymbol{\gamma}_\ell \in \mathbb{C}^{r\times 1}$ contains the related block-dependent weights.

B. LR Estimation Methods

The LR JST algorithm [16] performs the ML estimation of the ST MIMO channel from (6) under the LR constraint (12). The estimate, for known rank order r, is obtained as

$$\hat{\boldsymbol{h}}_{\mathrm{LR},\ell} = \hat{\boldsymbol{C}}^{\frac{\mathrm{H}}{2}}\hat{\boldsymbol{\Pi}}_{\mathrm{JST}}\hat{\boldsymbol{C}}^{-\frac{\mathrm{H}}{2}}\boldsymbol{h}_\ell = \hat{\boldsymbol{C}}^{\frac{\mathrm{H}}{2}}\hat{\boldsymbol{\Pi}}_{\mathrm{JST}}\tilde{\boldsymbol{h}}_\ell, \quad (13)$$

TABLE III: LR Channel Algorithms

Method	Correlation $\tilde{\mathbf{R}}$	Projector $\hat{\boldsymbol{\Pi}} = \boldsymbol{\Pi}_r(\tilde{\mathbf{R}})$
JST	$\tilde{\mathbf{R}}_{\mathrm{ST}}$	$\hat{\boldsymbol{\Pi}}_{\mathrm{JST}}$
DST	$\tilde{\mathbf{R}}_{\mathrm{T}}^{*} \otimes \tilde{\mathbf{R}}_{\mathrm{S}}$	$\hat{\boldsymbol{\Pi}}_{\mathrm{T}}^{*} \otimes \hat{\boldsymbol{\Pi}}_{\mathrm{S}}$
SST	$\tilde{\mathbf{R}}_{\mathrm{T}}^{*} \otimes \tilde{\mathbf{R}}_{\mathrm{S,TX}}^{*} \otimes \tilde{\mathbf{R}}_{\mathrm{S,RX}}$	$\hat{\boldsymbol{\Pi}}_{\mathrm{T}}^{*} \otimes \hat{\boldsymbol{\Pi}}_{\mathrm{S,TX}}^{*} \otimes \hat{\boldsymbol{\Pi}}_{\mathrm{S,RX}}$
LL-JST	$\tilde{\mathbf{R}}_{\mathrm{T}}^{*} \otimes \tilde{\mathbf{R}}_{\mathrm{S,TX}}^{*} \otimes \tilde{\mathbf{R}}_{\mathrm{S,RX}}$	$\tilde{\mathbf{U}}_{\mathrm{SST}}\hat{\boldsymbol{\Pi}}_{\mathrm{LLJST}}\tilde{\mathbf{U}}_{\mathrm{SST}}^{\mathrm{H}}$

by projecting the pre-whitened FR estimate $\tilde{\boldsymbol{h}}_\ell = \hat{\boldsymbol{C}}^{-\mathrm{H}/2}\hat{\boldsymbol{h}}_\ell$ onto the subspace spanned by the r leading vectors $\tilde{\mathbf{U}}_{\mathrm{JST}} = \mathrm{eig}_{\mathrm{r}}[\tilde{\mathbf{R}}_{\mathrm{ST}}]$ of the sample correlation matrix $\tilde{\mathbf{R}}_{\mathrm{ST}}$ defined in Table II, through the projector $\hat{\boldsymbol{\Pi}}_{\mathrm{JST}} = \boldsymbol{\Pi}_r(\tilde{\mathbf{R}}_{\mathrm{ST}}) = \tilde{\mathbf{U}}_{\mathrm{JST}}\tilde{\mathbf{U}}_{\mathrm{JST}}^{\mathrm{H}}$.

The computational cost of JST depends on the eigen-decomposition (EVD) of $\tilde{\mathbf{R}}_{\mathrm{ST}}$ which becomes unfeasible for practical (latency-constrained) mmWave systems as the correlation matrix is $N_{\mathrm{R}}N_{\mathrm{T}}W \times N_{\mathrm{R}}N_{\mathrm{T}}W$ and the number of blocks required for its estimation is $L \gg N_{\mathrm{R}}N_{\mathrm{T}}W$ [14]. In the following, this problem is addressed by proposing suboptimal methods that reduce the computational burden by decoupling the ST subspace into orthogonal domains of lower dimensions and by exploiting cascade filtering approaches. All methods are summarized in Table III.

1) Doubly-Space Time Estimator (DST): The DST method [14] assumes a separable ST structure for the channel correlation $\tilde{\mathbf{R}}_{\mathrm{ST}}$, as reported in Table III (second row). This assumption simplifies the projector into $\hat{\boldsymbol{\Pi}}_{\mathrm{DST}} = \hat{\boldsymbol{\Pi}}_{\mathrm{T}}^{*} \otimes \hat{\boldsymbol{\Pi}}_{\mathrm{S}}$ with $\hat{\boldsymbol{\Pi}}_{\mathrm{T}} = \boldsymbol{\Pi}_{r_{\mathrm{T}}}(\tilde{\mathbf{R}}_{\mathrm{T}})$ and $\hat{\boldsymbol{\Pi}}_{\mathrm{S}} = \boldsymbol{\Pi}_{r_{\mathrm{S}}}(\tilde{\mathbf{R}}_{\mathrm{S}})$. The spatial and temporal sample correlation matrices, $\tilde{\mathbf{R}}_{\mathrm{S}}$ and $\tilde{\mathbf{R}}_{\mathrm{T}}$ respectively, as well as the rank orders, r_{S} and r_{T}, are defined in Table II, where $\tilde{\mathcal{H}}_\ell = \mathrm{vec}^{-1}(\tilde{\boldsymbol{h}}_\ell)$ is the whitened FR channel estimate rearranged into a matrix of dimensions $N_{\mathrm{R}}N_{\mathrm{T}} \times W$ (see Table I). The rank orders represent the number of resolvable angles (r_{S}) and delays (r_{T}). This approach simplifies the computation to the EVD of two separate correlation matrices of lower dimensions compared to JST, i.e. $N_{\mathrm{R}}N_{\mathrm{T}} \times N_{\mathrm{R}}N_{\mathrm{T}}$ and $W \times W$.

2) Separate-Space Time (SST) Estimator: A novel method herein proposed to further reduce the complexity as well as the latency is based on the extension of the separable structure assumption to the spatial MIMO correlation $\tilde{\mathbf{R}}_{\mathrm{S}}$ as detailed in Table III (third row), according to the MIMO Kronecker model [21]. This simplifies the projector into $\hat{\boldsymbol{\Pi}}_{\mathrm{SST}} = \hat{\boldsymbol{\Pi}}_{\mathrm{T}}^{*} \otimes \hat{\boldsymbol{\Pi}}_{\mathrm{S,TX}}^{*} \otimes \hat{\boldsymbol{\Pi}}_{\mathrm{S,RX}}$ with $\hat{\boldsymbol{\Pi}}_{\mathrm{S,RX}} = \boldsymbol{\Pi}_{r_{\mathrm{S,RX}}}(\tilde{\mathbf{R}}_{\mathrm{S,RX}})$ and $\hat{\boldsymbol{\Pi}}_{\mathrm{S,TX}} = \boldsymbol{\Pi}_{r_{\mathrm{S,TX}}}(\tilde{\mathbf{R}}_{\mathrm{S,TX}})$. The spatial correlations at the two sides of the MIMO link, $\tilde{\mathbf{R}}_{\mathrm{S,RX}}$ and $\tilde{\mathbf{R}}_{\mathrm{S,TX}}$, are defined in Table II, together with the spatial ranks, $r_{\mathrm{S,RX}}$ and $r_{\mathrm{S,TX}}$. The latters represent the number of angles that can be resolved by the TX and RX array, respectively. The $N_{\mathrm{R}} \times N_{\mathrm{T}}$ matrix $\tilde{\mathbf{h}}_\ell(w)$ is the whitened estimate of the MIMO channel for the w-th tap extracted from $\tilde{\mathcal{H}}_\ell$ according to (9). Notice that the projector computation reduces to the EVD of three matrices of dimentions $N_{\mathrm{R}} \times N_{\mathrm{R}}$, $N_{\mathrm{T}} \times N_{\mathrm{T}}$ and $W \times W$, and thus requires $L \ll N_{\mathrm{R}}N_{\mathrm{T}}W$.

3) Low-latency Low-complexity JST (LL-JST) Estimator: As shown in Sec. IV, the assumption of separable domains

of the DST and SST methods speeds up the convergence but limits the asymptotic performance of the LR estimator. For $L \to \infty$, in fact, the projection captures a subspace that includes the channel multipath components but also the noise laying in the intersections of the separate RX-TX space and time domains, as illustrated in Section III-B4. This leads to a higher error at convergence compared to JST. To guarantee both low latency/complexity and convergence to the optimal JST performance, we propose a new method that exploits the basis computed by the SST algorithm

$$\tilde{\mathbf{U}}_{\mathrm{SST}} = \tilde{\mathbf{U}}_{\mathrm{T}}^{*} \otimes \tilde{\mathbf{U}}_{\mathrm{S,TX}}^{*} \otimes \tilde{\mathbf{U}}_{\mathrm{S,RX}}, \tag{14}$$

to perform a further LR filtering in the subspace identified by SST. In (14) we set $\tilde{\mathbf{U}}_{\mathrm{T}} = \mathrm{eig}_{r_{\mathrm{T}}}[\tilde{\mathbf{R}}_{\mathrm{T}}]$, $\tilde{\mathbf{U}}_{\mathrm{S,TX}} = \mathrm{eig}_{r_{\mathrm{S,RX}}}[\tilde{\mathbf{R}}_{\mathrm{S,RX}}]$, and $\tilde{\mathbf{U}}_{\mathrm{S,TX}} = \mathrm{eig}_{r_{\mathrm{S,TX}}}[\tilde{\mathbf{R}}_{\mathrm{S,TX}}]$. We consider the $r_{\mathrm{S,RX}} r_{\mathrm{S,TX}} r_{\mathrm{T}} \times 1$ projection of the FR channel estimate onto this basis:

$$\hat{\boldsymbol{s}}_{\mathrm{SST},\ell} = \tilde{\mathbf{U}}_{\mathrm{SST}}^{\mathrm{H}} \tilde{\boldsymbol{h}}_{\ell} = \boldsymbol{s}_{\ell} + \boldsymbol{n}_{\mathrm{SST},\ell}, \tag{15}$$

which is the sum of the channel-related component $\boldsymbol{s}_{\ell} = \tilde{\mathbf{U}}_{\mathrm{SST}}^{\mathrm{H}} \boldsymbol{C}^{-\frac{\mathrm{H}}{2}} \boldsymbol{h}_{\ell}$ and the projected FR estimate error $\boldsymbol{n}_{\mathrm{SST},\ell} = \tilde{\mathbf{U}}_{\mathrm{SST}}^{\mathrm{H}} \boldsymbol{C}^{-\frac{\mathrm{H}}{2}} \triangle \boldsymbol{h}_{\ell}$, with $\triangle \boldsymbol{h}_{\ell} = \hat{\boldsymbol{h}}_{\ell} - \boldsymbol{h}_{\ell}$. Note that for $L \to \infty$ it is $\mathcal{R}(\tilde{\mathbf{U}}_{\mathrm{SST}}) \supseteq \mathcal{R}(\tilde{\mathbf{U}}_{\mathrm{JST}})$, as it is $\hat{\boldsymbol{C}} \to \boldsymbol{C}$ and the estimated bases tend to the true channel bases in the selected domain, e.g. $\tilde{\mathbf{U}}_{\mathrm{JST}} \to \boldsymbol{C}^{-\frac{\mathrm{H}}{2}} \mathbf{U}_{\mathrm{ST}}$. Thereby the rank-$r$ channel is entirely embedded in $\boldsymbol{s}_{\ell}$ while the residual $\boldsymbol{n}_{\mathrm{SST},\ell}$ is white and includes both the component laying in the channel subspace $\mathcal{R}(\tilde{\mathbf{U}}_{\mathrm{JST}})$ (which can no longer be removed) and the artifacts laying in the orthogonal subspace $\mathcal{R}(\tilde{\mathbf{U}}_{\mathrm{SST}}) \setminus \mathcal{R}(\tilde{\mathbf{U}}_{\mathrm{JST}})$ captured by the intersections of the three separate domains due to the SST Kronecker approximation. In order to remove these artifacts, we propose to apply the optimal JST approach to the rank-r signal $\hat{\boldsymbol{s}}_{\mathrm{SST},\ell}$ and therein identify the long-term channel subspace. The sample correlation:

$$\hat{\mathbf{R}}_{s} = \frac{1}{L} \sum_{\ell=1}^{L} \hat{\boldsymbol{s}}_{\mathrm{SST},\ell} \hat{\boldsymbol{s}}_{\mathrm{SST},\ell}^{\mathrm{H}}, \tag{16}$$

isolates the truly invariant channel structure, thus the subspace projector is $\hat{\boldsymbol{\Pi}}_{\mathrm{LLJST}} = \boldsymbol{\Pi}_{r}(\hat{\mathbf{R}}_{s})$ and the LL-JST estimate is:

$$\hat{\boldsymbol{h}}_{\mathrm{LR},\ell} = \hat{\boldsymbol{C}}^{\frac{\mathrm{H}}{2}} \tilde{\mathbf{U}}_{\mathrm{SST}} \hat{\boldsymbol{\Pi}}_{\mathrm{LLJST}} \hat{\boldsymbol{s}}_{\mathrm{SST},\ell}. \tag{17}$$

4) An illustrating example: The difference between the proposed LR methods is explained by an example focusing on the spatial structure only to ease the visualization. We consider a multipath channel composed of $P = 4$ resolvable paths described by 3 DOA $\psi_{p}^{\mathrm{RX}} = \{\pi/3, \pi/2, 2\pi/3\}$ and 3 DOD, $\psi_{p}^{\mathrm{TX}} = \{\pi/3, \pi/2, 2\pi/3\}$ such that 2 paths share the same DOA and 2 paths share the same DOD. This reduces the spatial diversity orders to $r_{\mathrm{S,TX}} = r_{\mathrm{S,RX}} = 3$ and $r_{\mathrm{S}} = 4$. The spatial structure of the channel is represented by plotting the power-angle-angle (PAA) diagram, assuming vertical arrays with $N_{\mathrm{R}} = N_{\mathrm{T}} = 16$.

Fig. 1 shows the PAA diagrams of (a) the channel, (b) the FR estimate, while (c) and (d) represent the LR projection

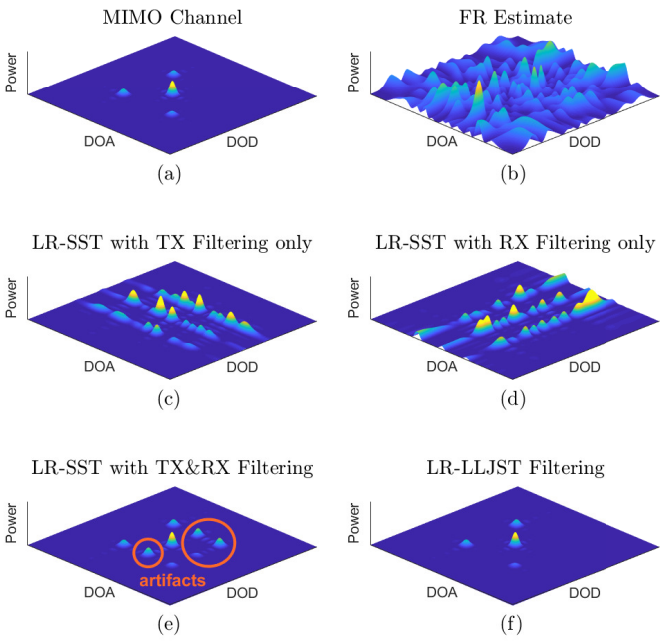

Fig. 1: PAA diagrams for different estimates of a MIMO multipath channel with degrees of spatial diversity $r_{\mathrm{S,TX}} = r_{\mathrm{S,RX}} = 3$ and $r_{\mathrm{S}} = 4$.

over the TX and RX domain, respectively. The Kronecker combination of the two filters by the SST method is in Fig. 1 (e) for optimal rank selection. Comparing Fig. 1 (a) and (e), it can be seen that the assumption of separable spatial structure leads to the selection of the PAA entries corresponding to $r_{\mathrm{S,TX}} r_{\mathrm{S,RX}}$ combinations of channel's DOA/DOD, introducing noise artifacts. On the other hand, the LL-JST method in Fig. 1 (f) is able to filter out these artifacts selecting only the channel components, reaching the same results of the JST approach, but with lower latency.

IV. Numerical Results

In this section we assess the (normalized) mean squared error (MSE) of the proposed estimation methods, i.e., $\mathrm{MSE} = \mathbb{E}[|\Delta \mathbf{h}_{\ell}|^2]/\mathbb{E}[|\mathbf{h}_{\ell}|^2]$, where $\mathbf{h}_{\ell} = [\mathbf{h}_{\ell}^{(1)} \cdots \mathbf{h}_{\ell}^{(N_{\mathrm{R}})}]$ and $\Delta \mathbf{h}_{\ell} = \mathbf{h}_{\mathrm{EST},\ell} - \mathbf{h}_{\ell}$, with $\mathbf{h}_{\mathrm{EST},\ell}$ denoting the generic $WN_{\mathrm{T}} \times N_{\mathrm{R}}$ estimated channel. In order to evaluate the performance against both interference and noise, the MSE is given as a function of the signal to noise and interference ratio $\mathrm{SINR} = \mathbb{E}[|\mathbf{h}_{\ell}|^2]/\mathbb{E}[|\hat{\mathbf{N}}_{\ell}|^2]$ evaluated at the output of the FR estimator, i.e. on signal (7), assuming optimal pilot sequences with diagonal $\mathbf{R}_{\mathrm{BB}}$. The noise covariance is modeled as $\mathbf{Q} = \sigma_{n}^2 \mathbf{I}_{N_{\mathrm{R}}} + \mathbf{Q}_{\mathrm{I}}$, where the two terms represent the RX noise and the interferers' contribution, respectively. We model the interferers as single rays impinging the RX array, thus

$$\mathbf{Q}_{\mathrm{I}} = \sum\nolimits_{i=1}^{N_{\mathrm{I}}} \Omega_{\mathrm{I},i} \sigma_{\mathrm{I},i}^2 \mathbf{a}^{\mathrm{RX}}(\boldsymbol{\theta}_{\mathrm{I},i}^{\mathrm{RX}}) \mathbf{a}^{\mathrm{RX}}(\boldsymbol{\theta}_{\mathrm{I},i}^{\mathrm{RX}})^{\mathrm{H}}, \tag{18}$$

where N_{I} is the total number of interferers, while $\sigma_{\mathrm{I},i}^2$, $\Omega_{\mathrm{I},i}$, and $\boldsymbol{\theta}_{\mathrm{I},i}^{\mathrm{RX}}$ represent the single interferer's transmitted power, path gain, and DOA, respectively. The signal to noise ratio (SNR) is the SINR in the absence of interference. We calculate

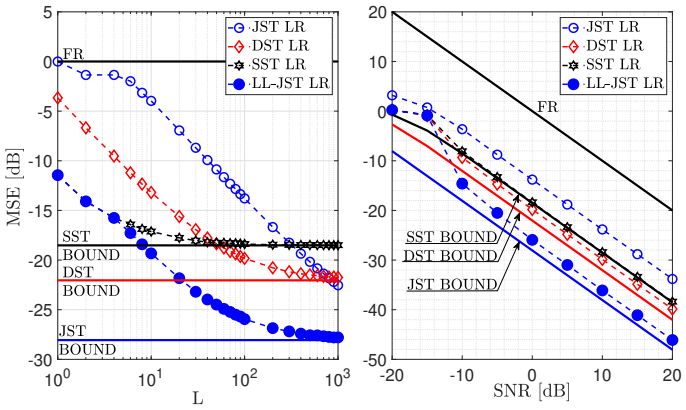

Fig. 2: MSE vs. L (left) and SNR (right) for LR channel estimation algorithms over a simplified non-line-of-sight (NLOS) channel with white noise.

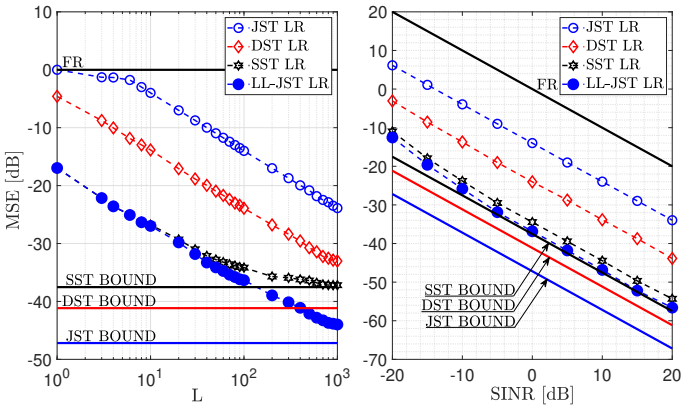

Fig. 3: MSE vs. L (left) and SINR (right) for LR channel estimation algorithms over simplified LOS channel with spatially correlated noise.

the lower bounds to the performance for each proposed method by extending the analysis in [5] from single-input-multiple-output (SIMO) to MIMO settings as detailed in [17]. We evaluate the algorithms' convergence rate by computing the MSE versus the number of slots L used for the estimation of the channel subspaces. The channel rank orders are estimated by means of the minimum description length (MDL) algorithm, as in [14].

The MIMO-OFDM system consists of two vertical uniform linear array (ULA)s, with $N_{\mathrm{R}} = 16$ and $N_{\mathrm{T}} = 16$ antenna elements and inter-element spacing $d = \frac{\lambda}{2}$, representing one line of a 16×16 planar array. Both the TX and RX devices use polarized antenna elements with polarization angles of $-45°$ and $45°$ for each array, respectively, and antenna gains as specified in Section 7.3 of [3]. The bandwidth is 100 MHz and the cascade of the TX and RX filters is a raised cosine with roll-off factor 0.2. The time-slot is 1 ms. The performance is over two different channels: simplified deterministic channels and 3GPP stochastic channels for urban macro cell (UMa) environment [3]. Note that all results are consistent with the array size (N_{R},N_{T}), and with the equivalent digital channel in case of hybrid analog/digital transceivers.

We first analyze the algorithms' performance on a simplified channel of 4 paths, in both LOS and NLOS conditions, with elevation angles $\left(\psi_p^{\mathrm{RX}}, \psi_p^{\mathrm{TX}}\right) = \{(115.2, 64.8), (145.2, 94.8), (85.2, 94.8), (85.2, 34.8)\}$ deg, for $p = 1, \ldots, 4$, respectively. With this choice, the spatial rank orders are: $r_{\mathrm{S,RX}} = 3, r_{\mathrm{S,TX}} = 3, r_{\mathrm{S}} = 4$. Path delays are set as $\tau_p = (p-1)T$, $p = 1, \ldots, 4$. Sampling is at symbol rate $1/T$, therefore the temporal rank is $r_{\mathrm{T}} = 4$, while $W = 10$. Normalized path powers are compatible with the distributions for the UMa channels in [3], including the antenna gains and the per-cluster shadowing, and are set as $\mathbf{\Omega}_{\mathrm{NLOS}} = [0.319, 0.272, 0.227, 0.182]$ for the simplified NLOS scenario, and $\mathbf{\Omega}_{\mathrm{LOS}} = [0.924, 0.030, 0.025, 0.021]$ for LOS one.

Fig. 2 (left) shows the LR algorithms' MSE performance against L for $\mathrm{SNR} = 0$ dB over the simplified NLOS channel, without interferers. All algorithms attain the corresponding lower bound, leading to a better estimation performance than the conventional unconstrained FR estimator. However, the four estimators converge at different rates: a larger number of slots is required by the JST method, due to the higher number of channel parameters to be estimated in the joint ST domain. The LL-JST outperforms all the other LR algorithms for $L > 4$, while for lower values, it is interestingly upperbounded by the SST algorithm. Within $L = 100$ slots, LL-JST has a MSE 2 dB higher than the asymptotic bound. Moreover, we observe that, despite of the lower asymptotic performances, the DST does not outperform the SST algorithm before $L = 50$ slots, while JST needs $L = 300$ and $L = 800$ slots to outperform the SST and DST algorithms, respectively, which can be critical for mmWave channels.

Fig. 2 (right) reports the MSE vs. SNR. All of the LR estimators provide a consistent gain with respect to the FR estimation, peaking at 26 dB with the LL-JST algorithm for most of the SNR values. Similarly as in the previous case, the LL-JST algorithm is upperbounded by the SST algorithm where the ratio between observations and noise becomes unfavorable, in this case $\mathrm{SNR} < -10$ dB.

Fig. 3 shows the MSE of LR algorithms over the simplified LOS channel, assuming the presence of 3 equally-powered interferers paths impinging the RX array, so that one interferer path is superimposed to one channel path, i.e., it has the same DOA as the channel's path, while the other interferers and channel's paths do not share the same DOAs. $\mathbf{Q}$ is assumed to be known. The performance against L is evaluated for $\mathrm{SINR} = 0$ dB. With respect to Fig. 2, we observe lower asymptotic bounds, as most of the interference is concentrated within directions that are well separated from the channel's DOAs. Since the convergence rate is similar, we observe that it takes more slots for all the algorithms to reach the convergence and within $L = 100$, only the SST is at 3 dB from its lower bound, while reaching the JST bound is possible within $L = 1000$ slots only for the LL-JST algorithm.

We now show the performance of the proposed estimation algorithms over the 3GPP stochastic channels, generated according to [3] assuming a UMa propagation environment,

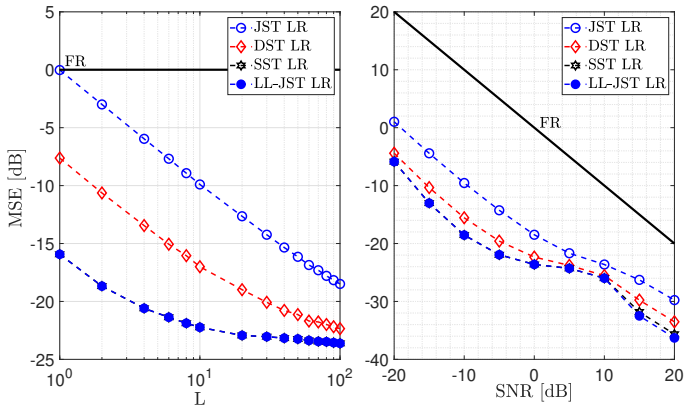

Fig. 4: MSE vs. L (left) and SNR (right) for LR channel estimation algorithms over 3GPP UMa-LOS channel with white noise.

white noise, and the worst-case synchronization error, with the first arrival placed between two sampling instants ($\tau_1 = 5.5T$). Fig. 4 reports the MSE performance. As for the simplified scenarios, all LR algorithms have a significant gain with respect the FR estimator, but faster rate of convergence due to the LR nature of the channel, despite the numerous clusters and rays. However, due to the fact the estimated ranks are very low, the LL-JST algorithm does not provide a significant gain with respect to the SST algorithm, and both reach gains of almost 25 dB with respect to the FR estimator. Within $L = 100$, only at $\mathrm{SNR} = \{15, 20\}$ it can be observed a slight gain between the two algorithms.

V. Conclusions

We have proposed a set of new computationally efficient LR estimation methods that take into account of the mmWave peculiarities. Estimated channel covariances over a few transmission periods are exploited to improve existing techniques for dynamic mmWave MIMO systems. Numerical results on both simple and well-established 3GPP models show the merit of the proposed solutions, providing remarkable gains up to 37 dB over the FR channel estimate, and gains from 5 to 25 dB over existing LR solutions, within 100 slots. Furthermore, the performances are compared to asymptotic MSE lower bounds for invariant angles/delays and time-varying fading, showing that the proposed LR methods attain the analytical bounds. In summary, the proposed LR method i) attains the asymptotic MSE bound within tens to hundred of training slots, and ii) is independent on the array calibration.

References

[1] T. S. Rappaport, J. N. Murdock, and F. Gutierrez, "State of the art in 60-GHz integrated circuits and systems for wireless communications," *Proceedings of the IEEE*, vol. 99, no. 8, pp. 1390–1436, Aug. 2011.

[2] S. Rangan, T. S. Rappaport, and E. Erkip, "Millimeter-wave cellular wireless networks: Potentials and challenges," *Proceedings of the IEEE*, vol. 102, no. 3, pp. 366–385, Mar. 2014.

[3] Tecnical report, "5G; study on channel model for frequencies from 0.5 to 100 GHz (3GPP TR 38.901 version 14.3.0 release 14)," 2018.

[4] R. W. Heath, N. González-Prelcic, S. Rangan, W. Roh, and A. M. Sayeed, "An overview of signal processing techniques for millimeter wave MIMO systems," *IEEE J. Sel. Topics of Signal Processing*, vol. 10, no. 3, pp. 436–453, April 2016.

[5] G. Soatti, A. Murtada, M. Nicoli, J. Gambini, and U. Spagnolini, "Low-rank channel and interference estimation in mm-Wave massive antenna arrays," in *EURASIP European Signal Processing Conf. (EUSIPCO)*, Sep. 2018, pp. 922–926.

[6] J. Rodríguez-Fernández and N. González-Prelcic, "Channel estimation for hybrid mmWave MIMO systems with CFO uncertainties," *IEEE Trans. Wireless Commun*, pp. 1–1, 2019.

[7] E. Vlachos, G. C. Alexandropoulos, and J. Thompson, "Wideband MIMO channel estimation for hybrid beamforming millimeter wave systems via random spatial sampling," *IEEE J. Sel. Topics of Signal Processing*, vol. 13, no. 5, pp. 1136–1150, Sep. 2019.

[8] J. Zhang and M. Haardt, "Channel estimation and training design for hybrid multi-carrier MmWave massive MIMO systems: The beamspace ESPRIT approach," in *EURASIP European Signal Processing Conf. (EUSIPCO)*, Aug 2017, pp. 385–389.

[9] H. Ghauch, T. Kim, M. Bengtsson, and M. Skoglund, "Subspace estimation and decomposition for large millimeter-wave MIMO systems," *IEEE J. Sel. Topics of Signal Processing*, vol. 10, no. 3, pp. 528–542, April 2016.

[10] C. K. Anjinappa, Y. Zhou, Y. Yapici, D. Baron, and I. Guvenc, "Channel estimation in mmWave hybrid MIMO system via off-grid Dirichlet kernels," 2019.

[11] K. Chen-Hu, D. T. M. Slock, and A. G. Armada, "Low-rank channel estimation for mm-wave multiple antenna systems using joint spatio-temporal covariance matrix," in *2019 IEEE Int. Conf. Commun. Workshops (ICC Workshops)*, May 2019, pp. 1–6.

[12] Y. Kim, H. Lee, P. Hwang, R. K. Patro, J. Lee, W. Roh, and K. Cheun, "Feasibility of mobile cellular communications at millimeter wave frequency," *IEEE J. Sel. Topics of Signal Processing*, vol. 10, no. 3, pp. 589–599, April 2016.

[13] M. Mezzavilla, M. Zhang, M. Polese, R. Ford, S. Dutta, S. Rangan, and M. Zorzi, "End-to-end simulation of 5G mmWave networks," *IEEE Commun. Surveys Tutorials*, vol. 20, no. 3, pp. 2237–2263, 2018.

[14] M. Nicoli, O. Simeone, and U. Spagnolini, "Multislot estimation of fast-varying space-time communication channels," *IEEE Trans. Signal Processing*, vol. 51, no. 5, pp. 1184–1195, May 2003.

[15] M. Brambilla, D. F. Pardo, and M. Nicoli, "Location-assisted subspace-based beam alignment in LOS/NLOS mm-wave V2X communications," in *2020 IEEE Int. Conf. on Commun. (ICC): Signal Processing for Commun. Symposium (IEEE ICC'20 - SPC Symposium)*, Dublin, Ireland, Jun. 2020, pp. 1–6.

[16] M. Cicerone, O. Simeone, and U. Spagnolini, "Channel estimation for MIMO-OFDM systems by modal analysis/filtering," *IEEE Trans. Commun.*, vol. 54, no. 11, pp. 2062–2074, Nov 2006.

[17] A. Brighente, M. Cerutti, M. Nicoli, S. Tomasin, and U. Spagnolini, "Estimation of wideband dynamic mmWave and THz channels for 5G systems and beyond," *IEEE J. Sel. Areas Commun. Special Issue on Multiple Antenna Technologies for Beyond 5G*, p. to appear, 2020.

[18] O. E. Ayach, R. W. Heath, S. Abu-Surra, S. Rajagopal, and Z. Pi, "Low complexity precoding for large millimeter wave MIMO systems," in *IEEE Int. Conf. Commun. (ICC)*, June 2012, pp. 3724–3729.

[19] C. Lin and G. Y. Li, "Indoor Terahertz communications: How many antenna arrays are needed?" *IEEE Trans. Wireless Commun.*, vol. 14, no. 6, pp. 3097–3107, June 2015.

[20] I. Barhumi, G. Leus, and M. Moonen, "Optimal training design for MIMO OFDM systems in mobile wireless channels," *IEEE Trans. Signal Processing*, vol. 51, no. 6, pp. 1615–1624, 2003.

[21] D.-S. Shiu, G. J. Foschini, M. J. Gans, and J. M. Kahn, "Fading correlation and its effect on the capacity of multielement antenna systems," *IEEE Trans. Commun.*, vol. 48, no. 3, pp. 502–513, Mar. 2000.